Eur. Phys. J. B **19**, 281–287 (2001)

THE EUROPEAN PHYSICAL JOURNAL B

EDP Sciences

Magnetic circular dichroism in Co 2p photoemission of Co/Cu(1 1 13): Separation of the fundamental spectra

G. Panaccione[1,2,a], G. van der Laan[3], H.A. Dürr[3], J. Vogel[4], and N.B. Brookes[5]

[1] Istituto Nazionale per la Fisica della Materia, TASC Laboratory, 34012 Trieste, Italy
[2] Institut de Physique, Univ. Neuchâtel, 2001 Neuchâtel, Switzerland
[3] Magnetic Spectroscopy Group, Daresbury Laboratory, Warrington WA4 4AD, UK
[4] Laboratoire de Magnétisme Louis Néel, CNRS, 38043 Grenoble, France
[5] ESRF, BP 220, 38043 Grenoble, France

Received 26 September 2000

Abstract. We measured high-quality Co 2*p* magnetic circular dichroism (MCD) spectra in photoemission for > 5 ML Co films grown on Cu(1 1 13) using a "complete" experiment, where the sample magnetization and the light helicity vector were reversed separately. We show how the four measured spectra, $M^{\pm}P^{\pm}$, can be used to make new linear combinations, which correspond to the circular dichroism in the angular dependence (CDAD), magnetic linear dichroism in the angular dependence (MLDAD) and MCD spectra. The integrated signals of the MLDAD and CDAD can be used to estimate the error caused by the difference in the degrees of magnetization and light polarization, respectively, in the opposite alignments. The MCD signal integrated over the entire 2*p* region does not average to zero, as one would have expected from the sum rule for photoemission to a non-interacting continuum state. There is a strong MCD signal in the entire region between the $2p_{3/2}$ and $2p_{1/2}$ main lines with pronounced satellite structure. The differences between the measured and calculated results for an independent-particle and an atomic model indicate the presence of interatomic electron correlation effects and configurational mixing.

PACS. 75.30.Pd Surface magnetism – 75.25.+z Spin arrangements in magnetically ordered materials (including neutron and spin-polarized electron studies, synchrotron-source x-ray scattering, etc.) – 71.70.Ej Spin-orbit coupling, Zeeman and Stark splitting, Jahn-Teller effect – 79.60.-i Photoemission and photoelectron spectra

1 Introduction

The development of dedicated synchrotron-radiation beamlines with variable polarization insertion devices has enabled the exploitation of the soft X-ray region using magnetic dichroism techniques. Polarization-dependent spectroscopies have become an established tool to determine essential properties of the electronic structure of magnetic materials. Magnetic dichroism in photoemission from core levels has made an enormous progress since the first results in the early 90s by Baumgarten *et al.* [1] and Roth *et al.* [2] with circularly and linearly polarized X-rays, respectively. Further experiments, exploiting the angular dependence of the photoemission with its interference effects between the two emission channels, and theoretical studies in the framework of multipole-moment analysis [3,4] established the relationship between experimental setup and symmetry, *i.e.*, the chirality. With linearly polarized light the reversal of the magnetization direction in a plane perpendicular to the scattering plane (defined by light helicity vector and photoemission detector direction) corresponds to a symmetry inversion that gives rise to magnetic linear dichroism in the angular distribution (MLDAD). This inversion is essentially the same as obtained by reversing the circular polarization in a coplanar geometry, where light direction, magnetization and photoemission direction are in the same plane. In the latter case one obtains the magnetic circular dichroism (MCD), which in principle provides the same information about the magnetic ground state as MLDAD [3,5]. Within the fundamental-spectra theory, the shape of MLDAD and MCD are identical only for a *p* shell photoemission, which is the case of present work. However, small differences exist in *d* and *f* shell photoemission, due to higher-order contributions [6]. Similarly, circular dichroism in the angular distribution (CDAD) and magnetic linear dichroism (MLD) are related through symmetry principles. This means that it is important to be aware of any "hidden" chiralities in the experimental geometry since they can lead to spurious effects in the measured signals.

MLDAD and MCD have been observed for a wide range of magnetic systems. In localized systems, such

[a] e-mail: panaccioneg@elettra.trieste.it

as rare earths, many-body effects lead to a pronounced multiplet structure due to Coulomb and exchange interaction [7,8]. Although 3*d* transition metals (TM) are normally associated with itinerant magnetism, results from high-energy spectroscopies have shown that electron-correlation effects can play an important role, such as in the case of nickel metal [9,10]. This dual nature explains why the theoretical interpretation of MCD, MLDAD and CDAD has been developed using different approaches: on the one hand, the one-particle model [11–16] and on the other, the many-body approach [3,4,17–20]. Both models give an overall agreement with the experimental results, depending on the particular system. Magnetic dichroism from 3*d* TM 2*p* core levels is ideally suited for further investigation concerning the applicability of the different theoretical approaches, especially since the 2*p* spin-orbit splitting gives a large energy separation of the two main structures.

In this paper we present magnetic dichroism results obtained at the Co 2*p* core level of Co/Cu(1 1 13), where we demonstrate how to separate the different contributions arising from geometrical misalignment and instrumental asymmetries. By performing measurements under both magnetization and polarization reversal we obtain the true MCD signal, as well as small CDAD and MLDAD signals which can always be present in these experiments. The 2*p* MCD spectrum displays intense signals at the main lines accompanied by satellite features due to the configurational mixing in ground and final states.

2 Experiment and method

The Cu(1 1 13) single crystal was obtained from a cut of 6° off with respect to the Cu [1$\bar{1}$0] direction. Clean Cu surfaces were prepared in UHV conditions by several cycles of Ne^+ sputtering (700 eV) and subsequent annealing at 700 K. Details about the morphology of the crystalline stepped surface and growth of Co can be found elsewhere [21,24]. Deposition of Co was performed at a rate of ∼0.5 Å/min. in a vacuum better than 2×10^{-10} mbar. The film thickness was monitored both by a quartz balance and by the relative ratio of the photoemission peaks; we estimated an error of ∼10% in the thickness. Auger electron spectroscopy (AES) and X-ray photoelectron spectroscopy showed neither contamination (carbon, oxygen) nor Cu segregation. All evaporations and measurements were performed at room temperature. The as-grown films were remanently magnetized using a high-current pulse through a nearby coil. MCD-PE and X-ray magnetic circular dichroism [in absorption] (XMCD) measurements were performed on beamline ID12B of the European Synchrotron Radiation Facility (ESRF) at Grenoble. Circularly polarized radiation was provided by a helical undulator by phasing the horizontal and vertical magnetic fields in the device [25,26]. The overall energy resolution was 300 meV for PE and 200 meV for XMCD.

The Co 2*p* XMCD was used to verify the spin and orbital magnetic moments of the films by comparing them to the known values [21]. Thin Co films grown on Cu(1 1 13) display some particular magnetic properties, such as an enhanced orbital moment [21]. This is confirmed by the results shown in Figure 1, where the orbital to spin magnetic moment ratio, $m_{\rm orb}/m_{\rm spin}$, obtained by applying the XMCD sum rules [22,23], is plotted as a function of Co coverage. The dashed lines indicate the theoretical values for surface and bulk. We found that the curve in Figure 1 was useful as an extra check to control the thickness in the thin-layer region, while at the same time allowed a verification of the magnetic quality. For each fresh film we gradually increased the layer thickness until the $m_{\rm orb}/m_{\rm spin}$ value dropped to ∼0.14. This resulted in films slightly thicker than 5 ML, which were used for the PE measurements. Large modifications of the surface morphology due to the presence of terraces are expected to influence the electron confinement for several layers. Part of the results obtained relies on this influence, even if we consider that the 2*p* MCD-PE should be less sensitive to changes in the orbital moment than the 2*p* XMCD, where the core electron is excited directly into an empty 3*d* state.

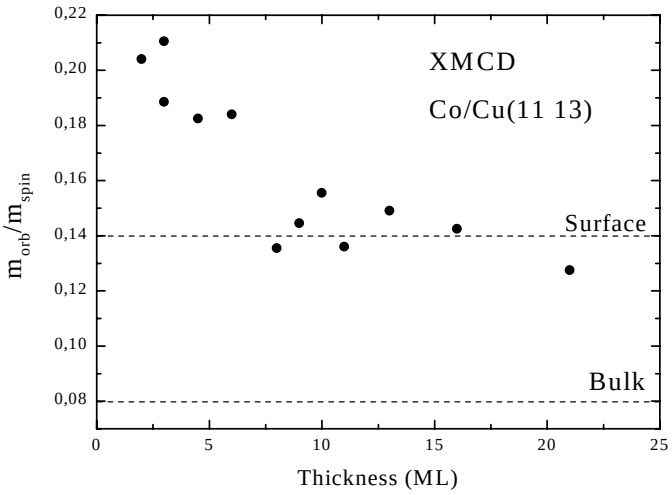

Fig. 1. Orbital to spin magnetic moment ratio as obtained from XMCD in absorption by applying the sum rules to the Co 2*p* level as a function of thickness for Co grown onto the Cu (1 1 13) surface. The dashed lines indicate the ratios for surface and bulk.

The PE was measured in remanence using essentially a non-chiral geometry: the photoelectrons were detected in the scattering plane, defined by the easy axis of magnetization (parallel to the surface steps [24]) and the incident radiation. PE spectra were measured by reversing the helicity of 85% circularly polarized X-rays ($P^{\pm}$) at fixed magnetization direction, as well as by reversing the magnetization ($M^{\pm}$) along the easy axis (parallel to the surface steps [24]) for fixed circular polarization. This results in four spectra, $M^{\pm}P^{\pm}$, which allows the analysis of a "complete" dichroism experiment.

Photoelectron diffraction (PED) effects, present at low kinetic energies [27], lead to intensity modulations as a function of photon energy and emission angle. These diffraction effects mix the different fundamental spectra, as described in Section 4 of reference [3], changing the line

shape and magnitude of the dichroic asymmetry [27,28]. To ensure that possible PED features were averaged out, photoelectrons were collected at normal emission using a hemispherical multichannel analyser with a large acceptance angle of 40° and using relatively large kinetic energies (100 to 200 eV).

3 Theory

The electric dipole transition probability for angular-dependent spin-integrated photoemission J in the direction $\hat{\varepsilon}$ for light with polarization $\hat{\mathbf{P}}$ from an atom with multipole moment along $\hat{\mathbf{M}}$ is given by the general expression [3]

$$4\pi J(\hat{\mathbf{M}}, \hat{\mathbf{P}}, \hat{\varepsilon}) = \sum_{xab} I^x \, U^{xab}(\hat{\mathbf{M}}, \hat{\mathbf{P}}, \hat{\varepsilon}) \, B^{cc'l}_{xab}, \qquad (1)$$

where B is a radial term which depends on the phase difference, $\delta_c - \delta_{c'}$, for excitation to the two continuum states with orbital momentum $c = l \pm 1$. Expressions for B in the atomic case are given in reference [29]. In presence of photoelectron diffraction, B can be developed in Green's functions. The I^x are the fundamental spectra containing the physical information. Each I^x produces a set of angular distributions U^{xab} where x, a, b are the moments of the atomic shell, the light and the photoelectron distribution, respectively. In this notation $a = 0$ means isotropic light; $a = 1$ denotes circular dichroism, which is the difference in intensities for left and right circularly polarized light with the helicity vector along $\hat{\mathbf{P}}$; and $a = 2$ denotes linear dichroism: the intensities for light polarized in two perpendicular directions perpendicular to $\hat{\mathbf{P}}$ minus twice the intensity for light polarized along $\hat{\mathbf{P}}$. The set of angular distributions is limited by the triangular condition $\{x, a, b\}$, where b is even.

Reversal of $\hat{\mathbf{M}}$ or $\hat{\mathbf{P}}$ gives rise to MCD. Interference between the two final state channels c and c' can lead to CDAD and MLDAD, which vanishes in the angular integrated spectrum. Since photoelectron detectors measure only a finite angular range, the true MCD signal can be difficult to obtain. We can, however, separate the fundamental spectra as follows:

(i) Circular dichroism (CD)

Reversal of $\hat{\mathbf{P}}$ means that $a = 1$ and $x = 0, 1, 2$ (p shell) limits xab to {110, 112, 212} so that

$$4\pi J_{\mathrm{CD}} = \underbrace{I^1 U^{110} B_{110} + I^1 U^{112} B_{112}}_{\mathrm{MCD}} + \underbrace{I^2 U^{212} B_{212}}_{\mathrm{CDAD}}. \quad (2)$$

The CD signal is obtained for given $\mathrm{M}^{\pm}$ by reversing the direction of $\hat{\mathbf{P}}$,

$$(\mathrm{M}^{\pm}\mathrm{P}^{+}) - (\mathrm{M}^{\pm}\mathrm{P}^{-}) \cong \mathrm{CDAD} \pm \mathrm{MCD}. \qquad (3)$$

(ii) Magnetic dichroism (MD)

Reversal of $\hat{\mathbf{M}}$ means that $x = 1$ and $a = 0, 1, 2$ (electric dipole radiation) limits xab to {110, 112, 122} so that

$$4\pi J_{\mathrm{MD}} = \underbrace{I^1 U^{110} B_{110} + I^1 U^{112} B_{112}}_{\mathrm{MCD}} + \underbrace{I^1 U^{122} B_{122}}_{\mathrm{MLDAD}}. \quad (4)$$

The MD signal for given $\mathrm{P}^{\pm}$ is obtained by reversing the direction of $\hat{\mathbf{M}}$,

$$(\mathrm{M}^{+}\mathrm{P}^{\pm}) - (\mathrm{M}^{-}\mathrm{P}^{\pm}) \cong \mathrm{MLDAD} \pm \mathrm{MCD}. \qquad (5)$$

From equations (3) and (5) we obtain

$$\begin{aligned}
&(\mathrm{M}^{+}\mathrm{P}^{+}) + (\mathrm{M}^{-}\mathrm{P}^{+}) - (\mathrm{M}^{+}\mathrm{P}^{-}) - (\mathrm{M}^{-}\mathrm{P}^{-}) \cong 2\ \mathrm{CDAD},\\
&(\mathrm{M}^{+}\mathrm{P}^{+}) - (\mathrm{M}^{-}\mathrm{P}^{+}) + (\mathrm{M}^{+}\mathrm{P}^{-}) - (\mathrm{M}^{-}\mathrm{P}^{-}) \cong 2\ \mathrm{MLDAD},\\
&(\mathrm{M}^{+}\mathrm{P}^{+}) - (\mathrm{M}^{-}\mathrm{P}^{+}) - (\mathrm{M}^{+}\mathrm{P}^{-}) + (\mathrm{M}^{-}\mathrm{P}^{-}) \cong 2\ \mathrm{MCD}. \quad (6)
\end{aligned}$$

Writing this in the more condensed form,

$$\begin{aligned}
&(\mathrm{M}^{+} + \mathrm{M}^{-})(\mathrm{P}^{+} - \mathrm{P}^{-}) \cong 2\ \mathrm{CDAD},\\
&(\mathrm{M}^{+} - \mathrm{M}^{-})(\mathrm{P}^{+} + \mathrm{P}^{-}) \cong 2\ \mathrm{MLDAD},\\
&(\mathrm{M}^{+} - \mathrm{M}^{-})(\mathrm{P}^{+} - \mathrm{P}^{-}) \cong 2\ \mathrm{MCD}, \qquad (7)
\end{aligned}$$

these results can also be understood intuitively. The MCD is the difference between the spectra with $\hat{\mathbf{M}}$ and $\hat{\mathbf{P}}$ parallel and antiparallel. The MLDAD is the difference between the spectra with opposite directions of $\hat{\mathbf{M}}$ summed over the two helicity directions of the circular polarization. Thus the remaining effect must be due to linear polarization. Finally, the CDAD is the difference between the spectra with opposite directions of $\hat{\mathbf{P}}$ summed over the magnetization directions. By deriving equation (6) from the general expression for the angular dependent photoemission we have shown that there are no other contributions and that the parts in equations (2) and (3) which give the MCD contribution are the same.

Equation (6) shows that in general we need all four spectra to obtain the MCD. In a non-chiral atomic geometry we have that $U = 0$ for odd $(x + a + b)$ so that the CDAD and LMDAD vanish and only two spectra are required to determine the MCD. This is the conventional approach [1]. However, photoelectron scattering and misalignment can introduce additional CDAD and LMDAD contributions in an apparently coplanar geometry. This can lead to a distortion of the observed spectral shape.

4 Possible sources of error

In order to perform the measurements as accurate as possible, it is importance to know the possible – but usually unavoidable – sources of error.

First of all, in order to quantify the limit of our experimental set-up, we used the PE signal from the Cu 2*p* core level in the non-chiral geometry to obtain the differences of the four spectra, $\mathrm{M}^{\pm}\mathrm{P}^{\pm}$. For this *intrinsic instrumental asymmetry* we obtained a value of 5×10^{-3}. It takes

into account that the helicity reversal can change the footprint of the beam and its position, the photon flux and the photon energy. Furthermore, reversal of the applied magnetic field can magnetize parts of the electron analyser or its neighbourhood. However, the latter problems can normally be avoided by using non-magnetic components.

Since copper is non-magnetic the above provides no check on the differences in the degree of circular polarization and magnetization. Both the polarization and the magnetization might be slightly different for the two alignments, which gives rise to a *false* difference signal. These *external instrumental asymmetries* are setting the level of accuracy of the *true* signal. The precise degree of polarization depends on the optical path through the optical system of the beamline and might even be energy dependent. Also reversal of the applied magnetic field does not necessarily result in a perfect reversal of the sample magnetization, although the problems anticipated in this case are better to control than those of the light polarization.

For photoemission to a non-interacting continuum state, the intensity of each of the fundamental spectra, such as MCD, MLDAD and CDAD, integrated over the entire range should be equal to zero [29]. This holds as a consequence of the sum rules, since a continuum state far above the Fermi level has zero spin and orbital moments. The four spectra allow us to estimate the errors due to differences in sample magnetization for the two magnetization directions and differences in the degree of polarization for left and right circular polarization. If we define $m^{\pm}$ as the degree of sample magnetization for $M^{\pm}$ magnetization and $p^{\pm}$ as the degree of circular polarization for $P^{\pm}$ polarization (where $p^{\pm}$ and $m^{\pm}$ can attain values between 0 and 1), we obtain the integrated intensities, ρ, of the spectra as

$$\frac{\rho_{\mathrm{CDAD}}}{\rho_{\mathrm{ISO}}} = \frac{p^+ - p^-}{p^+ + p^-}, \tag{8}$$

$$\frac{\rho_{\mathrm{MLDAD}}}{\rho_{\mathrm{ISO}}} = \frac{m^+ - m^-}{m^+ + m^-}, \tag{9}$$

$$\frac{\rho_{\mathrm{MCD}}}{\rho_{\mathrm{ISO}}} = \frac{(m^+ - m^-)}{(m^+ + m^-)} \frac{(p^+ - p^-)}{(p^+ + p^-)} \,. \tag{10}$$

Here, we have made the assumption that the integrated difference spectra vanish when $m^+ = m^-$ and $p^+ = p^-$, which is only approximately correct when spurious effects are present, as will be discussed in Section 5.1 From equations (8–10) it is clear that the error for MCD is much smaller than for CDAD and MLDAD.

Further errors can occur due to *hidden* chiralities. These errors will be exposed when we make the linear combinations of equation (6). In an ideal in-plane geometry there is no chirality, but this can be induced by a small misalignment in sample mounting or by a miscut of the crystal. We can use the line shape of the dichroism spectra to decide whether we are dealing with a chiral effect. Both the MCD and MLDAD should have a characteristic $(-++-)$ shape [11]. The CDAD spectrum should have a $(-+-)$ shape for the $2p_{3/2}$ and a vanishing signal for the $2p_{1/2}$ level [11]. In the case of an external instrumental asymmetry we obtain a false MCD or MLDAD signal which will resemble the isotropic spectrum.

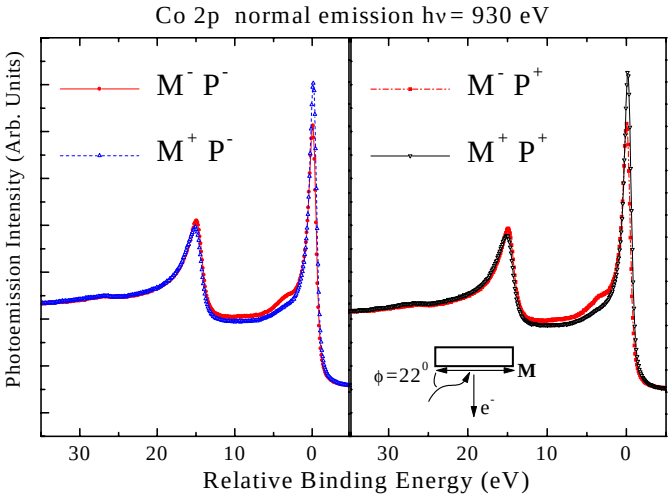

Fig. 2. The four Co $2p$ photoemission spectra with different alignment of magnetization and light helicity ($M^{\pm}P^{\pm}$) measured at a photon energy of $h\nu = 930$ eV in normal emission from > 5 ML Co/Cu(1 1 13). The insert shows the experimental geometry. The zero of the relative binding energy scale is taken at the maximum of the isotropic spectrum.

5 Results and discussion

5.1 Error limitations

Figure 2 shows the four different Co $2p$ PE spectra, $M^{\pm}P^{\pm}$, measured at $h\nu = 930$ eV in normal emission. The high quality of the data reveals strong satellite structures at the high-binding energy sides of the $2p_{3/2}$ and $2p_{1/2}$ main lines. In order to analyse the dichroism we make the new linear combinations given in equation (6). Figures 3 and 4 show the result for the MCD, CDAD and MLDAD obtained from the four Co $2p$ spectra measured at $h\nu = 1000$ eV. The integrated intensities are obtained as $\rho_{\mathrm{CDAD}}/\rho_{\mathrm{ISO}} = 0.5\%$ and $\rho_{\mathrm{MLDAD}}/\rho_{\mathrm{ISO}} = 0.1\%$. Therefore, using equations (8–10) we deduce that the external instrumental asymmetry for the MCD is smaller than 0.05%. However, the value measured for $\rho_{\mathrm{MCD}}/\rho_{\mathrm{ISO}}$ in Figure 3 is much larger. It amounts to a value up to 5% depending on the geometry and film thickness, which confirms previous findings [30]. These values are far outside the error bar. Since the photoemission was collected in a very wide acceptance angle, PED effects can be eliminated as a possible cause. The significant non-zero integrated intensity suggests that also other effects might contribute to the dichroism. Spin filtering comes to mind as one of the possible reasons for a non-zero integrated intensity [11]. This effect is known to be important for secondary electrons with a low-kinetic energy, where the inelastic mean free path is spin-dependent [31,32]. It should be small for

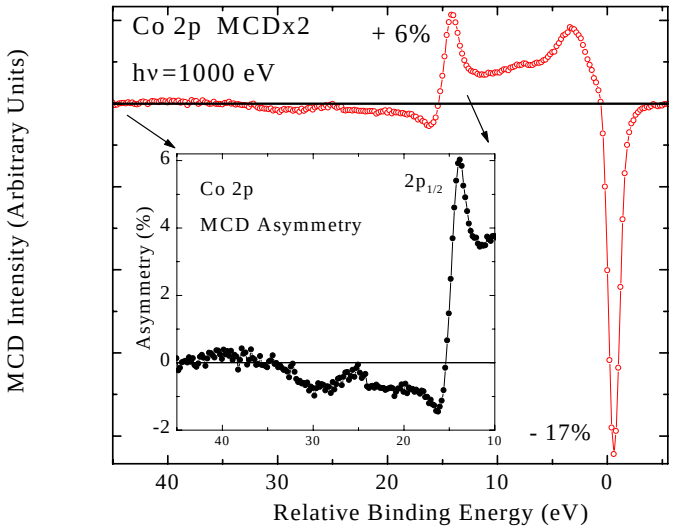

Fig. 3. Co 2*p* MCD obtained from the four photoemission spectra measured at $h\nu = 1000$ eV from > 5 ML Co/Cu(1 1 13). Values of the MCD asymmetry on the main lines are indicated. The insert shows the region near the $2p_{1/2}$ in more detail, plotting the asymmetry instead of the difference. Three wiggles arising from the satellites can be distinguished showing ∼1% magnetic asymmetry.

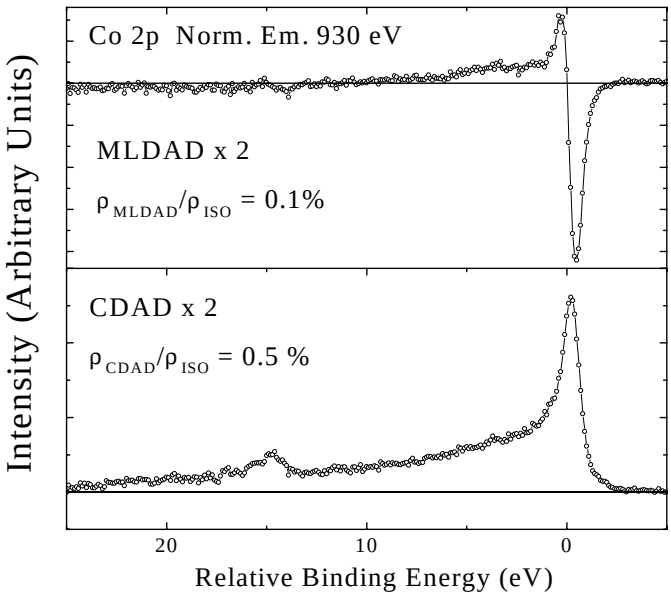

Fig. 4. Co 2*p* MLDAD and CDAD obtained from the four photoemission spectra in Figure 2. The values of the integrated intensity ratios are indicated.

primary photoelectrons, but might be present in the background of the secondary electrons. Results on TM with spin polarized 2*p* PE suggest that the background for majority and minority channel cannot be superimposed at both sides of the spectrum, leaving a net difference in the two channels at the high binding energy side [33]. In the absence of a better explanation it is tempting to ascribe the non-zero integrated intensity in the measured dichroism to a residual spin effect. Note that this spin effect is not expected to show up in CDAD and MLDAD.

The CDAD and MLDAD shown in Figure 4 are much smaller than the MCD in Figure 3. The maximum MLDAD peak to peak asymmetry value is less than 1%, which is near the limit of the experimental error bar. The ratio of the integrated intensity for MLDAD obtained from equation (9) is around 0.1%. Errors in estimating such small values are possibly due to the error in normalising the spectra, *i.e.* in aligning the intensity before and after the edges: in our case, spectra are obtained on a large kinetic energy scale, up to 20–30 eV before the $2p_{1/2}$ edge, in order to minimize this error. Theoretically, one expects the MLDAD to have a similar line shape as the MCD, which is roughly confirmed by experimental data. Therefore, the MLDAD is likely due to a small misalignment in the experimental geometry, creating a chiral geometry. The measured CDAD has a line shape which resembles the isotropic spectrum rather than the expected theoretical curve. This points to a difference in polarization for the two opposite helicities, which comes on top of the misalignment in the experimental set-up. Results obtained as a function of emission angle and thickness show a reduction of CDAD (up to a factor of three) going from normal incidence to normal emission, independent of the Co coverage. This excludes PED effects and confirms the misalignment, as evidenced by the MLDAD.

5.2 MCD structure

Our measurements are primarily aimed at obtaining the MCD, which in the chosen experimental geometry is far more accurate than the CDAD and MLDAD. The maximum of the MCD asymmetry, defined as the difference divided by the sum signal [28], is −17% at the $2p_{3/2}$ main line in Figure 3. Satellites at the high binding energy side give rise to broad structures in the positive dichroism of the $2p_{3/2}$ line and a dichroic tail for the $2p_{1/2}$ line. Closer inspection of the MCD asymmetry (insert of Fig. 3) reveals three wiggles that are clearly outside the experimental error bar. A remarkable feature is that the dichroism remains strong over the entire region between the two main lines. This region represents almost 40% of the total dichroic signal, partly arising from the satellites above the $2p_{3/2}$ edge. Previous 2*p* MLDAD measurements on Co and Fe metal revealed similar features [34–36] but in our case the satellite contribution is also enhanced in the isotropic spectrum (*cf.* Fig. 2). Accounting for differences in the kinetic energy dependence of MLDAD and MCD, this enhancement seems to be related to the difference in magnetic ground state of the Co film when grown on a stepped surface.

The origin of the satellite structure can be investigated using theoretical model calculations. Figure 5 shows a comparison between the measured MCD and calculated results for an independent-particle model and an atomic model. In the independent-particle model, the spin-polarized *d* electrons give an effective exchange field on the core level, resulting in a small splitting of the magnetic

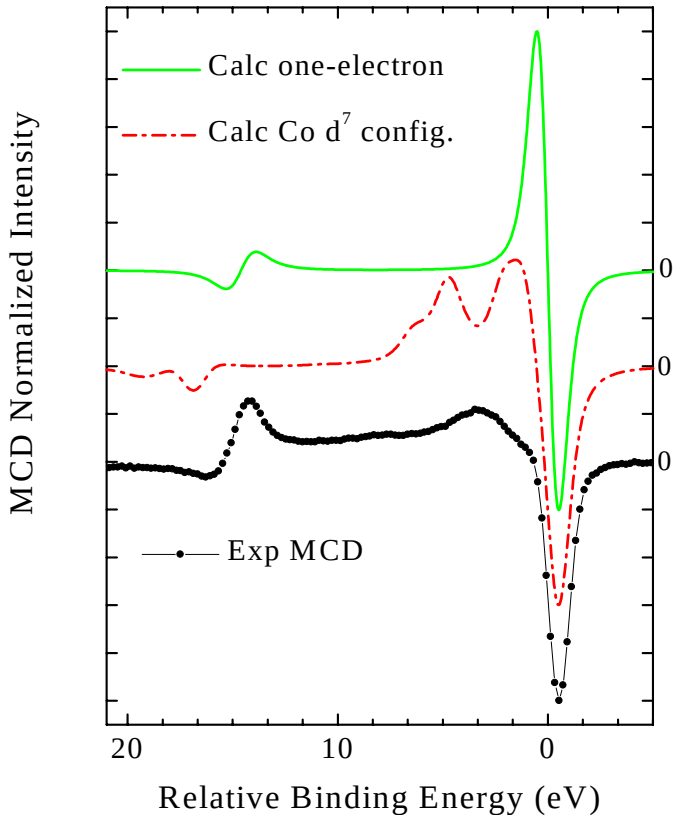

Fig. 5. Experimental Co $2p$ MCD-PE (bottom curve) from Figure 3 compared with calculated results for the independent-particle model (upper curve) and the atomic calculation (middle curve) for the Hund's rule ground state of Co d^7 with Hartree-Fock Slater integrals reduced to 80% (*cf.* Fig. 4b, I^{10} in reference [17]). The calculated spectra were broadened with a Lorentzian of $\Gamma = 0.5$ (1.0) eV for the $2p_{3/2}$ ($2p_{1/2}$) intrinsic width and a Gaussian of $\sigma = 0.3$ eV for the experimental resolution. The three spectra have been shifted vertically for clarity.

sublevels with a $(-+)$ and $(+-)$ line shape for the $2p_{3/2}$ and $2p_{1/2}$, respectively [11]. Each j level has an equal amount of spin-down states at high-binding energy as spin-up states at low-binding energy and *vice versa*. Since the exchange field on the core level is small, the dichroism vanishes in the region between the two edges. The experimental result (bottom curve) reveals the presence of an imbalance in the population of spin down and spin-up states, resulting in a net asymmetry in the dichroic signal. The core hole state appears to contain more spin-up than spin-down states. This effect can be due to spin filtering, as described in Section 5.1, or due to a difference in screening for the two spin states, as described in reference [30].

The calculation for the Hund's rule ground state, Co $3d^7\ {}^4F_{9/2}$, in Figure 5 shows that the atomic multiplet structure extends up to ∼8 eV above the $2p_{3/2}$ edge [17] but does not explain the dichroism observed at higher energies above this edge. When aligned to the main peak the atomic multiplet structure gives the impression of increasing the apparent core spin-orbit splitting. Thus neither the one-electron model nor the single-configurational atomic model are giving a perfect agreement with the experimental results. This points us in the direction of effects that are not included in these calculations, such as electron-correlation effects due to configurational mixing. The importance of electron correlation has recently been demonstrated for the Ni $2p$ MCD-PE, which gives a very good agreement with an impurity model calculation [37,38].

6 Conclusions

We have demonstrated that it is important to use the four spectra with reversed sample magnetization and light helicity, *i.e.* M^+P^+, M^-P^+, M^+P^- and M^-P^-, to make new linear combinations which give the CDAD, MLDAD and MCD. The method allows to estimate the experimental errors and has been applied to thin Co films grown on Cu(1 1 13). Even in a "non-chiral" geometry to measure the MCD, there can be small CDAD and MLDAD signals.

The measured Co $2p$ MCD spectrum has been compared with results from a one-particle calculation. Contrary to the calculated results, the measured spectrum shows a strong dichroism in the region between the $2p_{3/2}$ and $2p_{1/2}$ edges with distinct satellite structure above the edges. The region above the $2p_{1/2}$ displays at least three satellite features with different dichroic asymmetries. The spectrum is also distinctly different from the multiplet structure obtained in a single-configurational atomic Hartree-Fock calculation. This suggests the presence of interatomic electron-correlation effects and configuration interaction, which are not included in either of the two calculations. It confirms recent findings for metallic nickel, where the Ni $2p$ MCD-PE structure was explained by an impurity-model calculation [38]. However, nickel metal is considered to be a borderline case between a localized and delocalized system; for Fe and Co metal such calculations are less straightforward. It is important to obtain a better understanding of the intensity distribution in the TM $2p$ MCD-PE since it might also occur in the $3p$, where the exchange interaction and spin-orbit interaction are of the same order of magnitude.

We have carefully determined the experimental errors occurring in the difference spectra. Firstly, by measuring Cu $2p$ spectrum we verified that the magnetic dichroism vanishes for a non-magnetic sample with the noise to signal ratio in the order of 0.5%. Secondly, the error due to the difference in the degrees of magnetization and light polarization for the opposite alignments was estimated from the integrated signal of the MLDAD and CDAD. This method relies on the fact that, by virtue of the sum rules, for opposite alignments with equal degrees of polarization the integrated signal of the dichroism spectrum should vanish. We were able to distinguish between external instrumental asymmetry and hidden chiralities. The good statistics of our spectra allows to confirm that the MCD integrated over the entire $2p$ region does not average to zero, which might be due to spin filtering or spin dependent screening.

References

1. L. Baumgarten, C.M. Schneider, H. Petersen, F. Schafers, J. Kirschner, Phys. Rev. Lett. **65**, 492 (1990).
2. Ch. Roth, F.U. Hillebrecht, H. Rose, E. Kisker, Phys. Rev. Lett. **70**, 3479 (1993); Ch. Roth, H. Rose, F.U. Hillebrecht, E. Kisker, Solid State Commun. **86**, 647 (1993).
3. B.T. Thole, G. van der Laan, Phys. Rev. B **49**, 9613 (1994).
4. B.T. Thole, G. van der Laan, Solid State Commun. **92**, 427 (1994).
5. G. Panaccione, P. Torelli, G. Rossi, M. Sacchi, F. Sirotti, G. van der Laan, Phys. Rev. B **58**, R5916, (1998).
6. G. Panaccione, P. Torelli, G. Rossi, F. Sirotti, P. Prieto, G. van der Laan, J. Phys. Cond. Matt. **11**, 3431 (1999).
7. G. van der Laan, E. Arenholz, E. Navas, A. Bauer, G. Kaindl, Phys. Rev. B **53**, R5998 (1996).
8. G. van der Laan, E. Arenholz, E. Navas, Z. Hu, E. Mentz, A. Bauer, G. Kaindl, Phys. Rev. B **56**, 3244 (1997).
9. T. Jo, G.A. Sawatzky, Phys. Rev. B **43**, 8771 (1991).
10. G. van der Laan, B.T. Thole, J. Phys. Cond. Matt. **4**, 4181 (1992).
11. G. van der Laan, Phys. Rev. B **51**, 240 (1995).
12. H. Ebert, L. Baumgarten, C. M. Schneider, J. Kirschner, Phys. Rev. B **44**, 4466 (1991).
13. J. Henk, A.M.N. Niklasson, B. Johansson, Phys. Rev. B **59**, 13986 (1999).
14. D. Venus, Phys. Rev. B **49**, 8821 (1994).
15. J. Bansmann, L. Lu, K.H. Meiwes-Broer, T. Schlathölter, J. Braun, Phys. Rev. B **60**, 13860 (1999).
16. E. Tamura, G.D. Waddil, J.G. Tobin, P.A. Sterne, Phys. Rev. Lett. **73**, 1533 (1944).
17. B.T. Thole, G. van der Laan, Phys. Rev. B **44**, 12424 (1991).
18. G. van der Laan, B.T. Thole, Phys. Rev. B **48**, 210 (1993).
19. G. van der Laan, M.A. Hoyland, M. Surman, C.F.J. Flipse, B.T. Thole, Phys. Rev. Lett. **69**, 3827 (1992).
20. G. van der Laan, B.T. Thole, Solid State Commun. **92**, 427 (1994).
21. H.A. Dürr, G. van der Laan, J. Vogel, G. Panaccione, N. B. Brookes, E. Dudzik, R. McGrath, Phys. Rev. B **58**, R11853 (1998).
22. B.T. Thole, P. Carra, F. Sette, G. van der Laan, Phys. Rev. Lett. **68**, 1943 (1992).
23. P. Carra, B.T. Thole, M. Altarelli, X. Wang, Phys. Rev. Lett. **69**, 2307 (1993).
24. A. Berger, U. Linke, H.P. Oepen, Phys. Rev. Lett. **68**, 832 (1992).
25. P. Elleaume, J. Synchrotron Radiat. **1**, 19 (1994).
26. M. Drescher, G. Snell, U. Kleineberg, H.-J. Stock, N. Müller, U. Heinzmann, N.B. Brookes, Rev. Sci. Inst. **68**, 1939 (1997).
27. F.U. Hillebrecht, H.B. Rose, T. Kinoshita, Y.U. Idzerda, G. van der Laan, R. Denecke, L. Ley, Phys. Rev. Lett. **75**, 2883 (1995).
28. G. Panaccione, F. Sirotti, G. Rossi, Solid State Commun. **113**, 373 (2000).
29. G. van der Laan, Phys. Rev. B **55**, 3656 (1997).
30. H.A. Dürr, G. van der Laan, D. Spanke, F.U. Hillebrecht, N.B. Brookes, Europhys. Lett. **40**, 171 (1995).
31. H.C. Siegmann, in *Core Level Spectroscopies for Magnetic Phenomena: Theory and Experiment*, NATO-ASI Series B **345**, edited by P. Bagus, G. Pacchioni, F. Parmigiani (Plenum, New York, 1995), and references therein.
32. J.C. Gröbli, D. Oberli, F. Meier, Phys. Rev. B **52**, R13095 (1995).
33. F.U. Hillebrecht, Ch. Roth, H.B. Rose, W.G. Park, E. Kisker, N.A. Cherepkov, Phys. Rev. B **53**, 12182 (1996).
34. D.P. Pappas, G.D. Waddil, J.G. Tobin, J. Appl. Phys. **73**, 5936 (1993).
35. C.M. Schneider, U. Pracht, W. Kuch, A. Chassé, J. Kirschner, Phys. Rev. B **54**, 15618 (1996).
36. G. Rossi, G. Panaccione, F. Sirotti, S. Lizzit, A. Baraldi, G. Paolucci, Phys. Rev. B **55**, 11488 (1997).
37. G. van der Laan, S.S. Dhesi, E. Dudzik, J. Minar, H. Ebert, J. Phys. Cond. Matt. **12**, L275 (2000).
38. G. van der Laan, S.S. Dhesi, E. Dudzik, Phys. Rev. B **61**, 12277 (2000).